Available online at www.sciencedirect.com

ScienceDirect

journal homepage: www.intl.elsevierhealth.com/journals/dema

Titanium dioxide and modified titanium dioxide by silver nanoparticles as an anti *biofilm* filler content for composite resins

Hércules Bezerra Dias[a], *Maria Inês Basso Bernardi*[b], *Taís Maria Bauab*[c], *Antônio Carlos Hernandes*[b], *Alessandra Nara de Souza Rastelli*[a,*]

[a] *Department of Restorative Dentistry, Araraquara School of Dentistry, University of São Paulo State — UNESP, Araraquara, SP 14801-903, Brazil*

[b] *Department of Physics and Materials Science, Physics Institute of São Carlos — IFSC, University of São Paulo – USP, São Carlos, SP 13566-590, Brazil*

[c] *Department of Biological Sciences, Pharmaceutical Sciences School, University of São Paulo State — UNESP, Araraquara, SP 14801-902, Brazil*

ARTICLE INFO

Article history:
Received 4 March 2018
Received in revised form 9 July 2018
Accepted 1 November 2018

Key-words:
Titanium dioxide
Nanoparticles
Composite resin
Streptococcus mutans
Biofilms

ABSTRACT

Objective. The aim of this study was to evaluate the antibacterial activity of a composite resin modified by TiO_2 and TiO_2/Ag nanoparticles and their influence over different properties.

Methods. TiO_2 and TiO_2/Ag NPs were synthesized by polymeric precursor and microwave-assisted hydrothermal methods and then, characterized by different techniques. Direct contact test was performed using Filtek™ Z350XT blended with 0.5; 1 and 2% (wt.) of NPs against *Streptococcus mutans* to determine the best concentration to the other tests. After that, the modified composite resin was tested against *S. mutans* 7-day biofilm (CFU/mL). Also, compressive and diametral tensile strength ($n = 40$), degree of conversion ($n = 25$) and surface roughness ($n = 50$) was performed. The data were analyzed by ANOVA and Tukey's test for multiple comparison at 5% significance level.

Results. The direct contact test demonstrates that by increasing the nanoparticle content, the bacterial growth is significantly reduceed ($p < 0.05$). The inclusion of 2% of TiO_2/Ag NPs significantly decreased ($p < 0.05$) the biofilm accumulation of *S. mutans* on the composite resin surface compared to the control Group. The TiO_2 NPs treated with an organosilane increased compressive strength of composite resin ($p < 0.05$). Degree of conversion remained unchanged ($p > 0.05$) and the surface roughness increased with the NPs ($p < 0.05$), except for the TiO_2 by polymeric precursor Group ($p > 0.05$).

Significance. The development of an antibacterial dental restorative material that hinder *S. mutans* biofilm without sacrificing the mechanical and physical properties is desirable in dental material science.

* *Corresponding author at*: University of São Paulo State — UNESP, Araraquara School of Dentistry, Department of Restorative Dentistry, 1680 Humaitá St., P.O. Box 331, Araraquara, São Paulo, 14801-903, Brazil.
E-mail address: alrastelli@foar.unesp.br (A.N. de Souza Rastelli).

https://doi.org/10.1016/j.dental.2018.11.002

1. Introduction

A broad-spectrum antimicrobial composite resin materials is desired for dentistry, especially because composite resin materials accumulate more biofilm than other restorative materials and the current dental restorative materials did not have antimicrobial materials in the composition [1,2]. The high biofilm accumulation by composite resin restoration can contributes to the progress of secondary caries [3]. Because of that, researchers have focused their studies on nanostructured materials with antimicrobial potential, such as silver [4,5], zinc oxide [6,7], titanium dioxide [8,9], hydroxyapatite and chlorhexidine, in order to fabricate a novel resin based restorative material.

Metal oxides and silver doped metal oxides have been reported to show high antimicrobial activity and these metal oxides can be obtained by several chemical methods, which can provide different sizes and shapes [6]. Although, the metal oxides show proper antibacterial activity [7], under nanometric size the antibacterial effect is mainly attributed to their large surface area, allowing a great presence of atoms on the surface, which provides the maximum contact of the particles with the external environment [10,11]. Additionality, the small size of these particles facilitates the penetration through cell membranes, changing the intracellular processes that result in increased reactivity and antimicrobial activity [11,12].

Titanium dioxide (TiO_2) is one of the most studied metal oxide considered as an antibacterial, is a photocatalyst material that occurs mainly as two important polymorphs: the stable rutile phase and the metastable anatase [13]. These structures exhibit different properties and, consequently, different photocatalytic performances [13,14]. With the decrease of particle size, especially smaller than 50 nm, they have photoinduced activities, releasing energy that can be expressed chemically as free radicals and that can be applied in photocatalytic activities including the killing of bacteria and viruses [13,15,16].

In order to improve the antibacterial activity of Ag NPs and meanwhile to cut down the expense, a bunch of Ag containing complex materials have been developed and have been used as another approach to dental materials modification [17]. Ghosh et al. [18] synthesized ZnO/Ag nanohybrid employing chitosan as mediator by purely electrostatic interaction and verified that the synergistic antibacterial effect of ZnO/Ag nanohybrid on Gram-positive and Gram-negative bacteria is found to be more effective, compared to the individual components (ZnO and Ag). Zhang et al. [17] synthesized Ag islands on ZnO, by a two-step preparation using a self-catalytic reaction and verified that the antibacterial activity of Ag/ZnO NPs, especially with 5.0 wt.% of Ag, against *Escherichia coli* and *Staphylococcus aureus* was greatly enhanced in contrast with the simple mixture of Ag and ZnO NPs. The authors attributed this enhancement to the obvious increase in the reactive oxidative species (especially superoxide) and the increased damage to plasmid DNA induced by Ag/ZnO NPs [17]. Zamperini et al. [5] synthesized and characterized hydroxyapatite nanoparticles decorated with silver and evaluated the antifungal effect of these nanoparticles in distilled water solution against *Candida albicans*. These authors found an interaction between the structure and the defect density variation in the interfacial Ag decorated NPs and intrafacial pure NPs region with the fungal medium resulted in fungistatic and fungicidal activity.

Although the incorporation of metal nanoparticles and metal oxides into dental composites provides antimicrobial activity, they might adversely affect the physical and mechanical properties [4–7]. Another disadvantage could be the poor color stability obtained in materials containing metal nanoparticles, making this property probably clinically unacceptable in the case of aesthetic materials [19].

In this way, the purpose of this study was to modify a commercial composite resin with TiO_2 and Ag decorated TiO_2 NPs in order to provide antibacterial capacity without sacrificing the mechanical and physical properties. The null hypothesis tested in the study is that the addition of small amounts of TiO_2 and Ag decorated TiO_2 NPs into a commercial composite resin do not affect the antibacterial activity, compressive and diametral tensile strength, surface roughness and degree of conversion.

2. Material and methods

2.1. *Experimental design*

This is an experimental study, which has dependent variables (5 levels) [compressive strength, diametral tensile strength, degree of conversion, surface roughness and antibacterial capacity (UFC/mL)] and independent variables [NPs concentrations (wt.%), synthesis method and type of NPs].

2.2. *Synthesis of TiO_2 NPs by polymeric precursor method (PREC POL)*

For synthesize TiO_2 NPs by polymeric precursor method [20], titanium isopropoxide ($Ti(OC_3H_7)_4$) (Sigma Aldrich P.A.) and citric acid ($C_6H_8O_7{\cdot}H_2O$, 99.5%) (Synth) were used as precursors. The ethylene glycol ($HOCH_2CH_2OH$, P.A. > 99,5%) (Synth) was added to polymerize the citrate by a polyesterification reaction. The citric acid:metal molar ratio was 3:1, while the citric acid:ethylene glycol (CA:EG) molar ratio was 60:40. The resulting resin was calcined at 300 °C for 4 h at 10 °C/min, leading to the formation of the precursors powder. The data of synthesized NPs are showed in Table 1.

Table 1 – Particle surface area and diameter calculated by BET data.

Material	Surface area BET (m^2/g)	Diameter by BET (nm)
TiO_2 PREC POL	58,02	24,44
TiO_2/Ag PREC POL	56,26	25,21
TiO_2 HYDROTH	322,58	4,40
TiO_2/Ag HYDROTH	447,60	3,17

Note: PREC POL = polymeric precursor method; HYDROTH = microwave assisted hydrothermal method.

2.3. Synthesis of TiO_2 NPs by microwave-assisted hydrothermal method (HYDROT)

For the preparation of TiO_2 nanoparticles by this method, 54 mL of the previously prepared titanium citrate precursor solution was taken into the reaction cup and 33.3 mL of NaOH was added to the precursor solution. The final solution filled out at least 90% of the total volume of the reaction cup in order to obtain maximum efficiency in relation to the self-generated pressure [21]. The reaction cup was inserted inside the reaction cell, it was closed and transferred to the microwave assisted hydrothermal system, where the reaction occurred at a heating rate of 140 °C min^{-1} and held at 140 °C for 10 min.

2.4. Silver decoration of the nanoparticles

The Ag decorated NPs were prepared using the previously prepared and TiO_2 powder dispersed in distilled water, and the pH was adjusted to 5 with HNO_3 [5]. The solution was stirred at 60 °C, and then 5 mL of $AgNO_3$ solution (1.4×10^{-2} M) was added in order to obtain a concentration of 1 mol NP:1 mol Ag. The precipitate was washed with distilled water until pH 7 and then dried in an oven.

2.5. Characterization of the nanoparticles

The X-Ray diffraction (XRD) patterns of the NPs powder were recorded on a Rigaku, Rotaflex RU200 B diffraction system with high intensity Cu Kα radiation (λ = 1.5406 Å), at 25 °C with 2θ values ranging from 20–80 °C and scanning rate of 0.02 °C per min. The crystallite size was determined by the following Scherrer equation where λ is the wavelength of the X-ray radiation, K is a constant taken as 0.89, θ is the diffraction angle and β is the full width at half maximum (FWHM).

$$D = \frac{K\lambda}{(\beta \cos\theta)} \quad (1)$$

The FTIR measurements of NPs were carried out in the Nexus 670 FTIR spectrophotometer (Thermo Scientific, Madison, WI). A total of 64 scans were collected from 4000 cm^{-1} to 650 cm^{-1} at 4 cm^{-1} resolution. Nitrogen adsorption–desorption measurements for the products were performed using a Micromeritics ASAP 2020 M + C instrument using Barrett–Emmett–Teller calculations for surface area determination. The isotherms and hysteresis curves were classified according to IUPAC (*International Union of Pure and Applied Chemistry*). The particle size (D_{BET}) was calculated using the following equation:

$$D_{BET} = \frac{6}{A_s.\rho} \quad (2)$$

where A is the superficial area (m^2/g) and ρ is the density of material (TiO_2 = 4,23 g/cm^3) JCPDF 73-1764.

The samples were structurally characterized using an automatic X-ray diffractometer (Rigaku, Ultima IV) with CuKα radiation (40 kV, 46 mA, θ = 1.5405 Å) and in a $\theta - 2\theta$ configuration using a graphite monochromator. The scanning range was between 20 and 80° (2θ), with a step size of 0.02° and a step time of 1.0 s.

The thermal decomposition processes were studied by thermogravimetry (TG, Netzsch STA 409C), in an oxygen atmosphere at a heating rate of 10 °C min^{-1}. Al_2O_3 was used as reference material during the thermal analysis.

The morphology and size of Ag decorated NPs were performed by transmission electron microscopy (TEM, Tecnai G2TF20, FEI).

The specific surface area (BET) and the diameter of NPs were estimated from the N_2 desorption/adsorption isotherms at liquid nitrogen temperature, using a Micrometrics ASAP 2020.

2.6. Composite resin used

The nanofilled composite resin Filtek™ Z350XT (3M Brazil) at color A_2B (Body) was employed as a control Group and modified by TiO_2 and TiO_2/Ag nanoparticles for experimental Groups.

2.6.1. Composite resin modification

The NPs were added into the composite resin Filtek™ Z350XT (3M Brazil) using a standardized protocol based on the inclusion of weight percentage of particles [22]. The NPs were incorporated into the composite resin mixing during 1 min, using a metal spatula and a glass plate. For direct contact test, the NPs were weighed corresponding to 0.5, 1 and 2% (wt.%). After the antibacterial screening, the specimens for the following tests were prepared with 2% (wt.%) of NPs.

2.7. Antibacterial assay for modified composite resin by TiO_2 nanoparticles

2.7.1. Bacterial strain and growing conditions

The *Streptococcus mutans* strain ATCC 25175 provided by Fio Cruz Foundation (Department of Microbiology, Reference Materials Laboratory, Sector Reference Bacteria located in the Oswaldo Cruz Foundation, National Institute of Health Quality Control – INCQS, Av Brazil , 4365 – Manguinhos, Cep: 21045-900, Rio de Janeiro, RJ, Brazil) was used. Initially, 3–5 colonies were collected from the Petri dish containing BHI agar (Brain Heart Infusion, Difco Laboratories, Becton Dickinson and Company, USA) + 1% sucrose, placed in a 15 mL falcon tube containing 5 mL Bacto™ BHI broth + 1% sucrose and incubated at 37 °C (± 1 °C) for 18 h. After growing, the bacterial culture was centrifuged (Excelsa® II Centrifuge, FANEM, Mod. 206 BL, serial number: HV 9462) at 3000 rpm for 15 min to obtain the pellet. The supernatant was discarded and the pellet resuspended in PBS (phosphate buffered saline) until reaching the absorbance of 0.08 read at 600 nm, with amount of cells of 10^8 CFU/mL using a spectrophotometer (Eppendorf AG, Hamburg, Germany). This suspension was used for the direct contact test and 7-days biofilm.

2.7.2. Direct contact test

The antibacterial activity of modified composite resin was tested by direct contact test [23]. The specimens were prepared immediately after composite resin modification as previously described. Specimens for antibacterial test were prepared using a stainless steel mold (4 mm in diameter and 2 mm in height). The split mold were placed on a glass slide and over-

filled with the composite resin containing TiO_2 and TiO_2/Ag NPs (0.5, 1 and 2% in weight). The holes of the mold were pressed with polyester strips and the top surface with another glass slide and specimens were light cured (LED Radii Plus — SDI, Australia) under 1500 mW/cm^2 for 40 s. The power output of the light-curing unit was measured using a Fieldmaster power meter (Coherent Commercial Products Division, model number FM, set n° WX65, part number 33-0506, USA) and the irradiance was calculated using the formula below:

$$I = \frac{P}{A} \quad (3)$$

where: I = irradiance or light intensity; P = power output and A = area of the light tip in cm^2.

After the photo-activation of 5 specimens for each test, the power output was checked.

For direct contact test, specimens were sterilized in an autoclave (121 °C/15 min) prior to the beginning of the test. The sterilized composite resin specimens were placed in a 24-well plate (Nunclon™, Nunc) and the wells were filled with 100 μL of *S. mutans* BHI suspension. They were incubated in an incubator at 37 °C in 10% of CO_2 for 1 h. After that, the wells were filled with 900 μL of BHI broth plus 1% sucrose and incubated at 37 °C for 18 h. The resultant suspensions of each well were submitted to ten-fold several dilutions until 1:100,000. A micropipette was used to retrieve 25 μL from each tube to spread on brain-heart infusion agar (BHI Agar, HiMedia Laboratories Pvt. Ltd., India) plates, which was incubated at 37 °C in 10% of CO_2 for 48 h, and then the colony forming units (CFU's) were counted.

The best concentration found in direct contact test against *S. mutans* was used to perform the antibacterial activity against *S. mutans* 7-days biofilm, physical and mechanical tests of modified composite resin in this study.

2.7.3. *Biofilm formation and bacterial counting*

The composite resin specimens (4 mm in height and 2 mm in diameter; n = 15) were placed in a 24-wells microculture plates (Nunclon™, Nunc) and the wells were filled with 100 μL of *S. mutans* BHI suspension plus 900 μL of BHI broth with 1% sucrose. Then, the plates were incubated at 37 °C (±1 °C) for 7 days. The BHI broth solution containing 1% of sucrose was replaced every 48 h. After 7 days, the BHI broth solution was removed, and the specimens were washed with sterile phosphate-buffered saline (PBS) for three times to remove non-adherent cells. The specimens were placed into sterile test tubes containing 5 mL of PBS (Phosphate-buffered saline) solution, stirring using a vortex for 1 min and immersed in an ultrasonic bath (Cristófoli Equipamentos de Biossegurança Ltda, Campo Mourão, Paraná, Brasil) during 5 min (room temperature; 42 kHz; 160 W). Serial dilution was performed using a micropipette to transfer 100 μL of this resultant solution to an Eppendorff® tube containing 900 μL of PBS, and then mix to obtain the first ten-fold solution until the last tube (1:100,000). Twenty-five microliters from each tube was retrieved to spread on brain-heart infusion agar (BHI Agar, HiMedia Laboratories Pvt. Ltd, India) plates, which were incubated at 37 °C (±1 °C) for 48 h, and then the colony forming units (CFU/mL) were counted.

2.8. *Compressive and diametral tensile strength tests*

According to ANSI ADA specification number 27 (American National Standard, 1993), the composite resin specimens for compressive (n = 40) (8 specimens for each Group) and diametral tensile strength (n = 40) (8 specimens for each Group) tests were prepared using a stainless steel split molds (4 mm in diameter and 8 mm in height). The specimens were light cured (LED Radii Plus — SDI, Australia) under 1500 mW/cm^2 on the top and bottom for 40 s and after removal from the mold, the photo-activation was also performed over the different sides of the specimens for the same time (total irradiation time of 1 min and 40 s). These specimens were stored in artificial saliva (Arte & Ciência, Araraquara, SP, Brazil, pH 7.0) and incubated (SPLabor, SP-200) at 37 °C for 24 h prior to the test.

The compressive strength was performed employing a mechanical test machine (DL2000, EMIC – Equipamentos e Sistemas de Ensaio Ltda., São José dos Pinhais, Paraná – Brazil) with a load cell of 5 kN at a cross-speed of 0.5 mm min^{-1}. For compressive assessment, the composite resin specimens were placed with their flat ends between the plates of the testing machine and the compressive load was applied along the long axis of the specimens. For diametral tensile strength assessment, the specimens were compressed diametrically introducing tensile stress in the material.

2.9. *Surface roughness test*

The reading of the surface roughness was obtained by the use of one 5 μm radius diamond tip of the portable surface roughness tester (Surftest Mitutoyo SJ-401, Mitutoyo Corporation, Japan) of 1 mm length, at a speed of 1 mm/s, with accuracy of 0.01 μm over the composite resin specimens (n = 50) (10 specimens for each group). This procedure was performed in three different places, creating three values that resulted in a final Ra average, which was calculated for each specimen. For the standardization of the readings, three equidistant lines were marked on the specimens in order to guiding the positioning of the diamond tip of the surface roughness tester to obtain the three reading points. The composite resin specimens were stored in artificial saliva (Arte & Ciência, Araraquara, SP, Brazil, pH 7.0) and incubated (SPLabor, SP-200) at 37 °C for 24 h prior to the test, and then reading of the initial roughness was performed (baseline reading) and final roughness reading was performed after 28 days of the immersion in artificial saliva.

2.10. *Degree of conversion measurements*

Fourier transform infrared (FTIR) spectroscopy was used to evaluate the degree of conversion (DC). The composite resin specimens were made and analyzed 24 h after the photo-activation. The light-cured composite resin specimens (n = 25), 5 specimens for each Group were pulverized into a fine powder. To prepare the pellet, 5 mg of the powder was mixed with 100 mg of potassium bromide powder (Merck, EMSURE®, ACS, Reag. Ph Eur; Lot K45884805) and then pressed to produce a thin pellet. The pellet was placed into a holder attachment into the spectrometer (Espectrum 2000, Perkin Elmer, USA). Uncured specimens (n = 25), 5 specimens for each Group were also mixed with potassium bromide powder and pressed to

obtain the pellets, as previously described. The measurements were recorded in the absorbance mode under the following conditions: 32 scans, a 4 cm^1 resolution and from 300 to 4000 cm^{-1} wavelength.

The degree of conversion was determined by the ratio of the absorbance intensities of aliphatic C=C peak at 1638 cm^{-1} against an internal standard peak of aromatic C=C at 1608 cm^{-1} before and after photoactivation. The DC (%) was determined by the following equation:

$$DC(\%) = \left\{1 - \frac{\left(1638\,cm^{-1}/1608\,cm^{-1}\right)\text{cured}}{\left(1638\,cm^{-1}/1608\,cm^{-1}\right)\text{uncured}}\right\} \times 100 \qquad (4)$$

2.11. *Statistical analysis*

The data was analyzed using the software IBM SPSS Statistics 20.0 (SPSS Inc. Chicago, USA). The normal distribution of the data was determined by Shapiro–Wilk test. Three-way ANOVA and Tukey's test for multiple comparisons were performed to direct contact tests and degree of conversion data. Two-way ANOVA and Tukey's test for multiple comparisons were performed for the antibacterial activity over the biofilm and mechanical tests. The Mauchly's sphericity test, a mixed model repeated measurements ANOVA and a post hoc test for repeated measures with adjustment of Bonferroni were performed for surface roughness test. All tests were performed at 5% significance level.

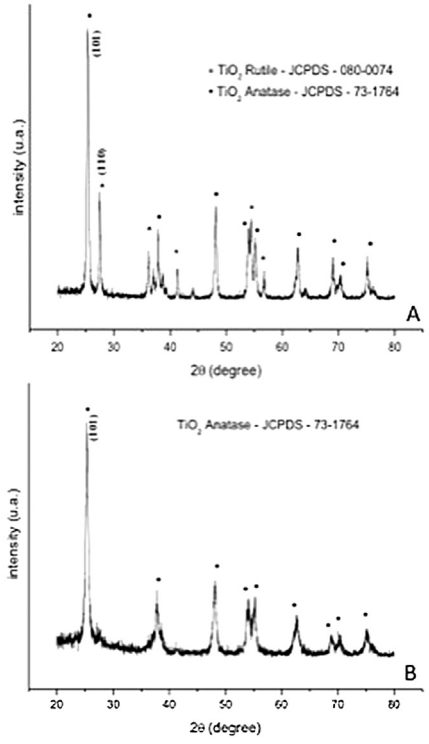

Fig. 1 – (A) XRD pattern of TiO_2 synthesized by polymeric precursor method. (B) XRD pattern of TiO_2 synthesized by hydrothermal method.

3. Results

The crystal structure and phase composition of TiO_2 was revealed by XRD analysis (Fig. 1A and B). The typical pattern showed is corresponding to crystalline TiO_2 powder (polymeric precursor) and the diffraction peaks could be indexed to anatase phase (JCPDS — 73-1764) as the main peak of the diffraction plane (101), in addition to rutile phase (JCPDS — 080-0074) with the main peak of the diffraction plane (110). Regarding the NPs obtained by microwave-assisted hydrothermal synthesis the pattern is consistent with pure anatase phase.

The Fig. 2A and B show the N_2 adsorption–desorption isotherms of the crystalline TiO_2 powder. The adsorption/desorption curve (hysteresis loop), in Fig. 2A and B, for TiO_2 NPs obtained by both synthesis presents typical of characteristic mesopores adsorbed with strong and weak affinity and with average pore diameter between 2–50 nm, considered H2 type according to the classification of IUPAC [24]. The TiO_2

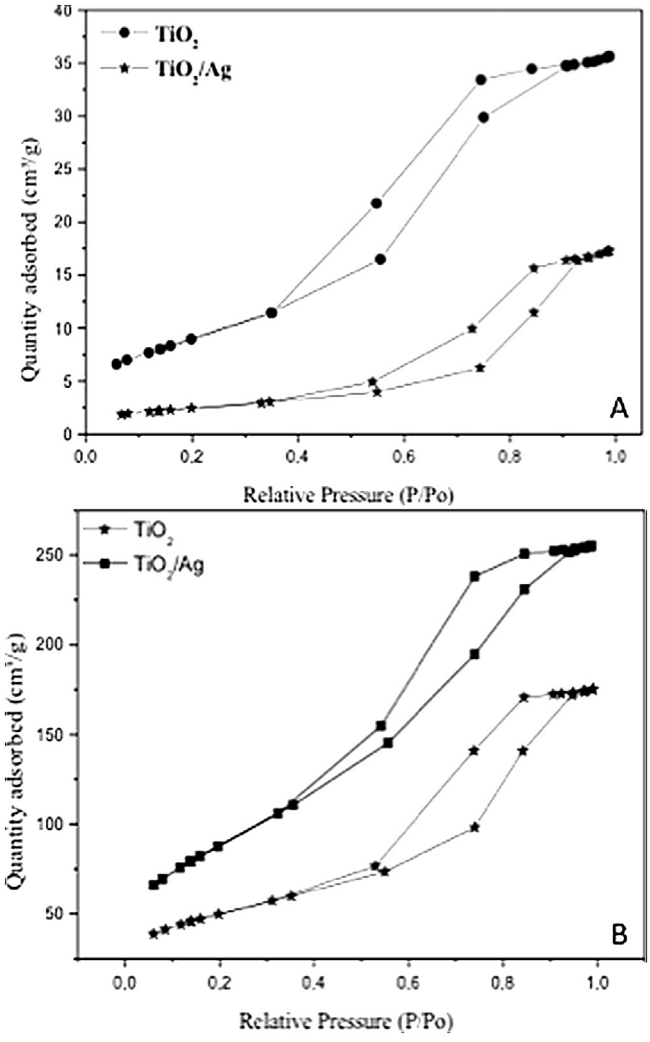

Fig. 2 – (A) N_2 adsorption–desorption isotherms of TiO_2 powder synthesized by polymeric precursor method. (B) N_2 adsorption–desorption isotherms of TiO_2 powder synthesized by hydrothermal method.

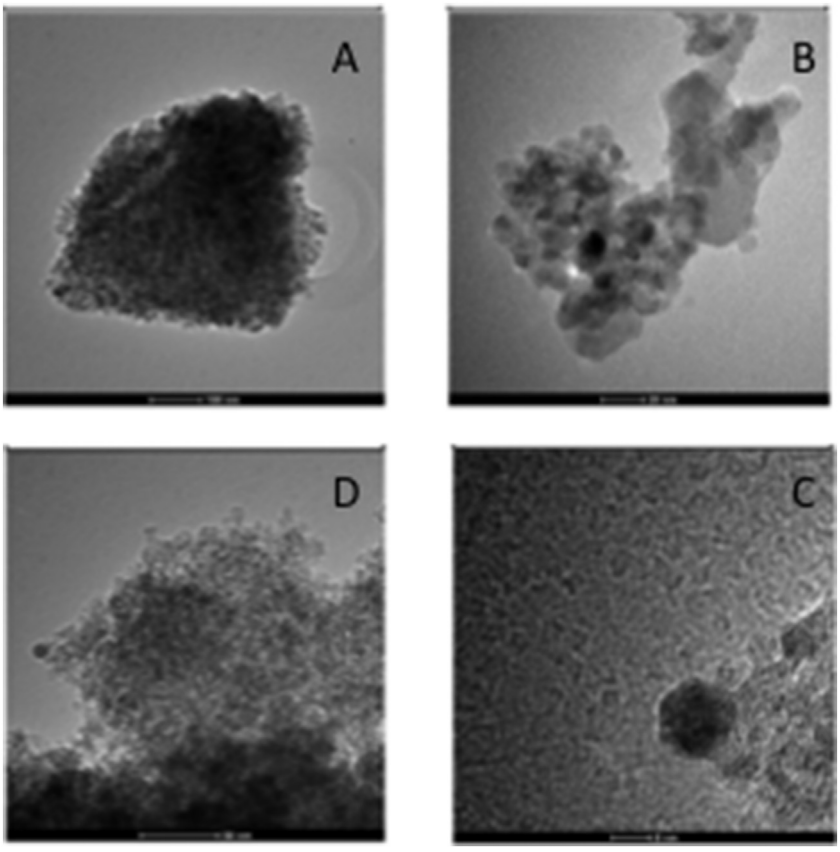

Fig. 3 – Transmission electron microscopy of Ag decorated TiO_2 synthesized by polymeric precursor (A–B) and hydrothermal methods (C–D).

and TiO_2/Ag NPs synthesized by hydrothermal synthesis presented the highest values of surface area and consequently the lowest values of average particle size, as can be seen in Table 1.

Fig. 3 shows the transmission electron microscopy of TiO_2/Ag synthesized by polymeric precursor and hydrothermal approach. Typical agglomerates of spherical nanoparticles with size ranging 5–10 nm were found to the NPs powder obtained by polymeric precursor and microwave-assisted hydrothermal synthesis.

The FT-IR spectrum representing the silanization pattern for the TiO_2 and TiO_2/Ag samples are showed in Fig. 4. After treatment of these NPs with TEVS, the absorption bands at 1007 and 1409 cm^{-1} indicating vibrational modes of SiO_2 bonds suggest that TiO_2 was successfully modified. The broad band with peak at 1012 cm^{-1} is relative to the Ti – O stretch.

The colony forming unit per mL (CFU/mL) for unmodified and modified composite resin by TiO_2 and TiO_2/Ag NPs (polymeric precursors technique) obtained by direct test are shown in Fig. 5A and B. The inclusion of 0.5, 1 and 2% by weight of TiO_2; 1 and 2% of TiO_2/Ag NPs (polymeric precursor) significantly inhibited ($p < 0.05$) the growth of *S. mutans* on the composite resin surface compared to the unmodified control Group. For the composite resin modified by TiO_2 and TiO_2/Ag NPs (hydrothermal technique), the results of CFU/mL are shown in Fig. 6A and B. The inclusion of 2% of TiO_2/Ag NPs significantly decreased ($p < 0.05$) *S. mutans* growth on the composite resin surface compared to the control Group. Based on the great antibacterial capacity of composite resin modified by 2% (weight), the following tests were performed using this concentration.

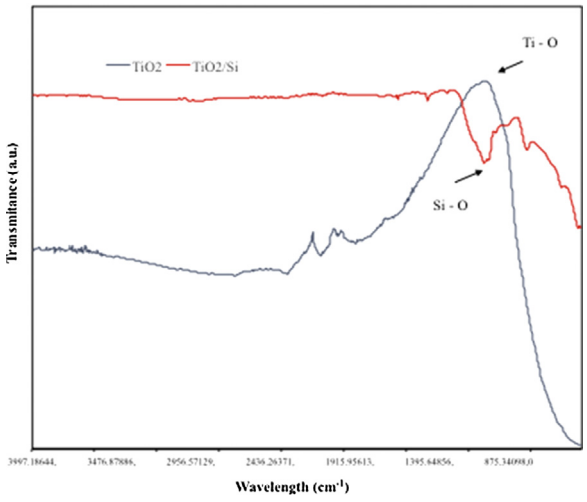

Fig. 4 – The FT-IR spectrum of the pure TiO_2 and TiO_2 modified by TEVS (triethoxyvinylsilane) (TiO_2/Si).

The colony forming unit per mL (CFU/mL) following 7-days *S. mutans* biofilm formation over unmodified and modified

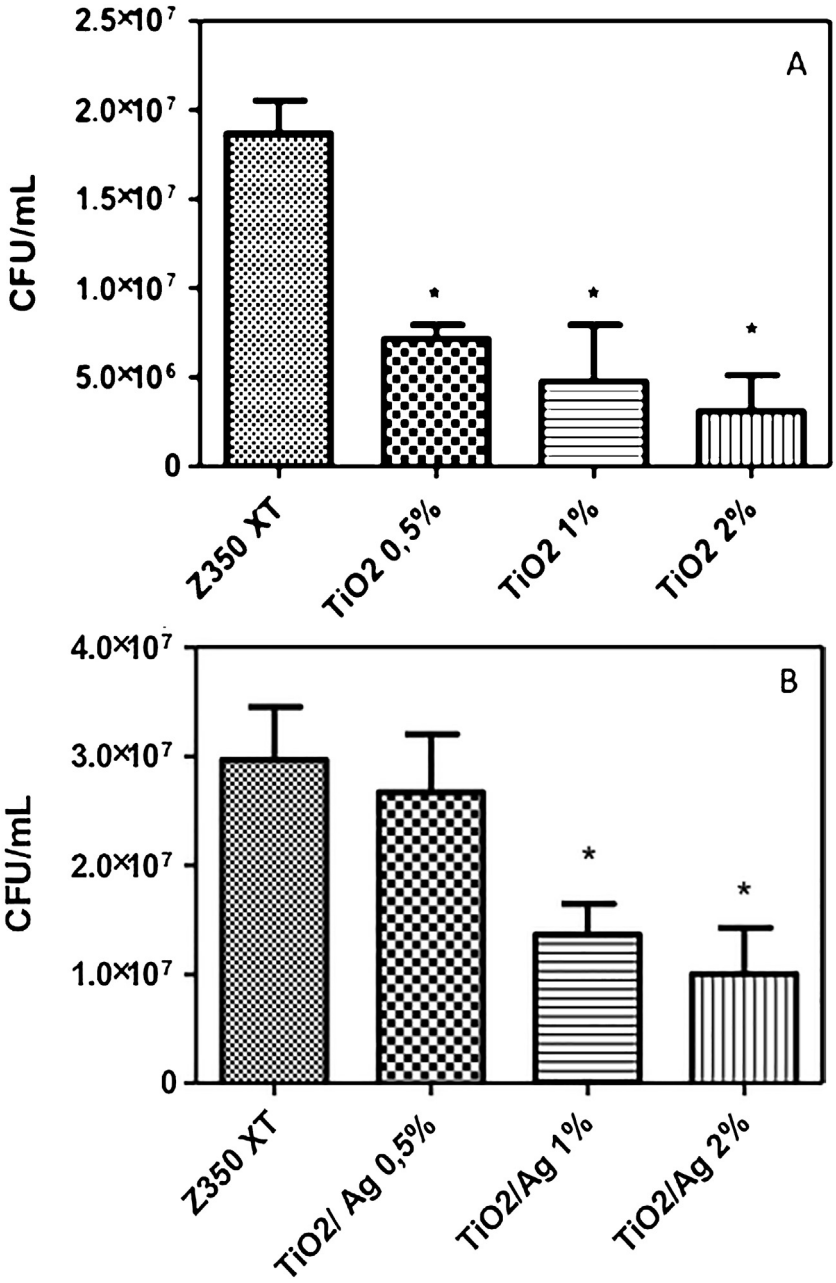

Fig. 5 – (A) Colony forming unit per mL (CFU/mL) following direct contact test for the unmodified (control Group) and modified composite resin by TiO_2 NPs (PREC POL) (% weight). *Indicate significant statistical differences comparing to unmodified resin composite ($p < 0.05$). (B) Colony forming unit per mL (CFU/mL) following direct contact test for the unmodified (control Group) and modified composite resin by TiO_2/Ag NPs (PREC POL) (% weight). *Indicate significant statistical differences comparing to unmodified resin composite ($p < 0.05$).

composite resin by 2% in weigth of TiO_2 and TiO_2/Ag NPs are shown in Fig. 7.

The degree of conversion (DC%) of unmodified and modified composite resin by 2% (weight) of TiO_2 and TiO_2/Ag NPs are presented in Table 2. Although the DC% value of composite resin modified by TiO_2 and TiO_2/Ag NPs are lower than unmodified resin, no significant differences were showed ($p > 0.05$) compared to control Group.

The mean values of the surface roughness (SR) over time of the composite resin Filtek™ Z350 XT modified by TiO_2 and TiO_2/Ag NPs are showed in Fig. 8. A mixed-model repeated measures ANOVA analysis for SR showed that the sphericity assumption was not met (after Mauchly test) for the Group in artificial saliva (Mauchly $W = 0.584$; $p < 0.001$). Adjustments for degrees of freedom were performed in order to correct these values. The general analysis showed no significant effect of repeated measures interaction with the tested Groups of modified composite resin ($p = 0.820$) on SR values over time (a within-subjects effect), indicating that the surface roughness of Filtek™ Z350 XT modified by the NPs was

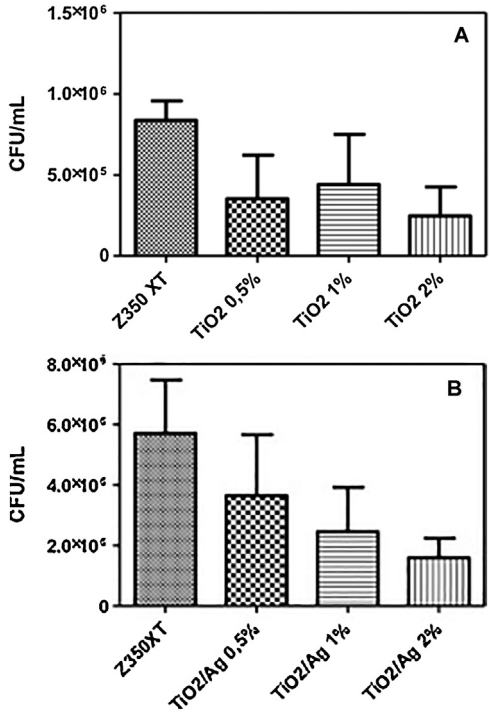

Fig. 6 – (A) Colony forming unit per mL (CFU/mL) following direct contact test for the unmodified (control Group) and modified composite resin by TiO_2 NPs (HYDROT) (% weight). *Indicate significant statistical differences comparing to unmodified composite resin ($p < 0.05$). (B) Colony forming unit per mL (CFU/mL) following direct contact test for the unmodified (control Group) and modified composite resin by TiO_2/Ag NPs (HYDROT) (% weight). *Indicate significant statistical differences comparing to unmodified composite resin ($p < 0.05$).

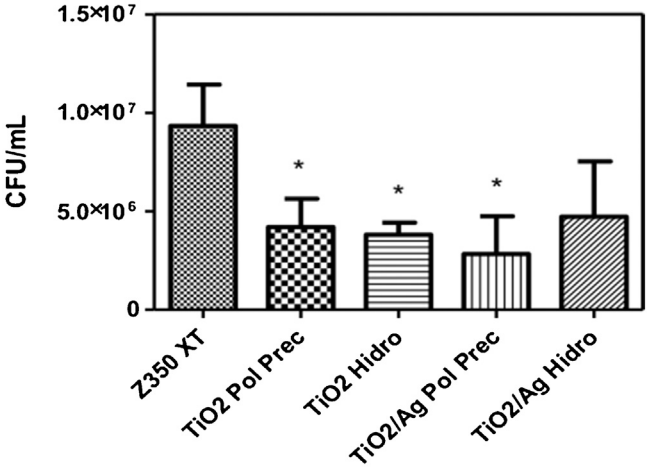

Fig. 7 – Colony forming unit per mL (CFU/mL) following 7-days *S. mutans* biofilm over unmodified (control Group) and modified composite resin by TiO_2 and TiO_2/Ag NPs (2% in weight). *Indicate significant statistical differences comparing to unmodified composite resin ($p < 0.05$). *Note*: PREC POL: polymeric precursor; HYDROT: hydrothermal.

Table 2 – Degree of conversion (%) of unmodified and modified composite resin by 2% (weight) TiO_2 and TiO_2/Ag NPs 59.2(1.0).

Material	Degree of conversion (%) and standard deviation (SD)
Z350 XT	59.2(1.0)[a]
TiO_2 PREC POL 2% (wt.)	49.6(3.2)[a]
TiO_2 HYDROT 2% (wt.)	51.8(2.7)[a]
TiO_2/Ag PREC POL 2% (wt.)	48.9(2.6)[a]
TiO_2/Ag HYDROT 2% (wt.)	57.3(1.9)[a]

Same superscript letters indicate no significant statistical diferences.
Note: PREC POL = polymeric precursor method; HYDROT = microwave assisted hydrothermal method.

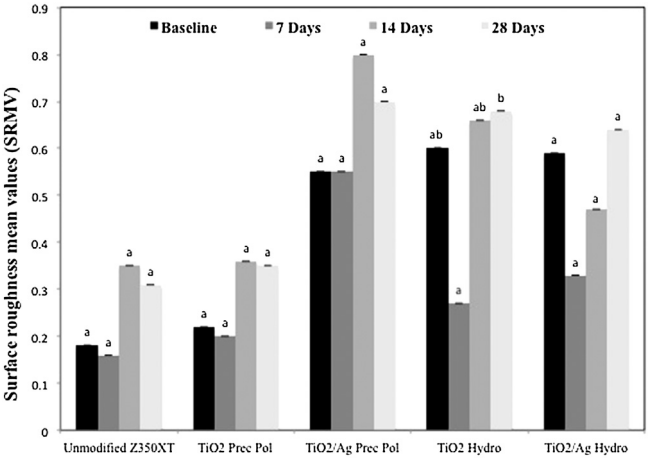

Fig. 8 – Surface roughness and standard deviation of unmodified and modified composite resin with TiO_2 and TiO_2/Ag NPs (2% in weight) over time. *Different superscript letters at the same line indicates significant statistical differences overtime. *Note*: PREC POL = polymeric precursor method; HYDROT = microwave assisted hydrothermal method.

not significantly affected over time. However, when the pairwise comparison based on estimated marginal means with Bonferroni adjustment showed that only the Group containing TiO_2 NPs (PREC POL) did not provide significant changes ($p = 1.00$) on composite resin SR compared to unmodified Group.

The mean values and standard deviation (MPa) for compressive strength and diametral tensile strength of unmodified and modified composite resin by TiO_2 and TiO_2/Ag NPs (wt.%) are showed in Figs. 9 and 10. The inclusion of 2% (wt.) of TiO_2 NPs (PREC POL) into the composite resin significantly increased ($p < 0.05$) the compressive strength of the composite resin compared to the unmodified Group.

4. Discussion

The synthesis obtained in this current study successfully provided nanosized materials according to Table 1 and Fig. 3,

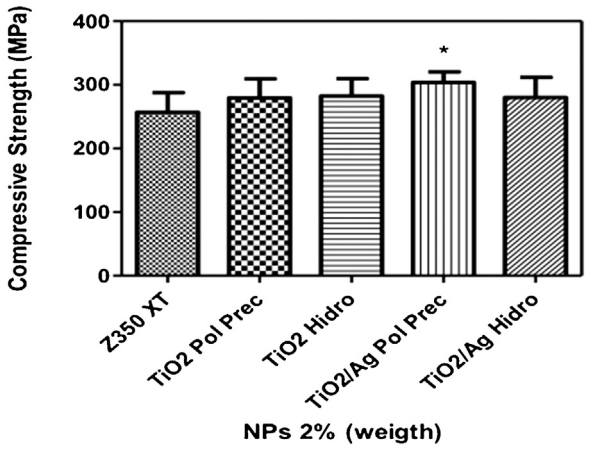

Fig. 9 – Compressive strength of modified composite resin by TiO_2 and TiO_2/Ag nanoparticles (wt.%). *Note*: PREC POL: polymeric precursor; Hydro: hydrothermal.

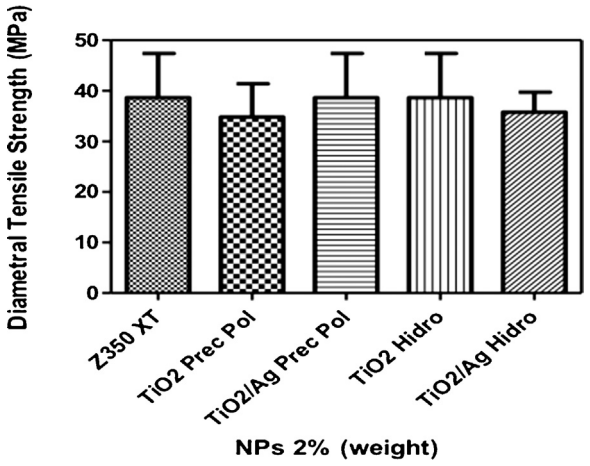

Fig. 10 – Diametral tensile strength of modified composite resin by TiO_2 and TiO_2/Ag nanoparticles (wt.%). *Note*: PREC POL: polymeric precursor; Hydro: hydrothermal.

with high surface area, which is an important characteristic for antibacterial activity, since it could enhance the contact of nanoparticles with cell membrane, contributing to the cell damage [10].

The results obtained in this study showed a significant antibacterial activity against *S. mutans* biofilm, both by direct contact test and against 7-days biofilm (Figs. 5–7). The nanoparticles obtained by hydrothermal synthesis with high surface area did not show a great antibacterial activity by direct contact test, however significantly hinder the growing of the 7-days biofilm. These findings could be related to the physical–chemical characteristics of the nanoparticles, such as synthesis route, size, shape and surface area. For the polymeric precursor method, based on the polymerization of the metal, the crystallinity of their products can be improved with increasing of EG:CA (ethylene glycol–citric acid monohydrate) mole ratio. [25]. On the other hand, the use of microwave irradiations during the synthesis have some advantages, which include efficient internal heating, increasing the temperature of the whole volume simultaneously and uniformly [26,27]. The ability to absorb microwave energy can vary in magnitude among different compounds, materials and metal oxides. can be successfully synthesized in different sizes and shapes by microwave synthesis 4.4 [26]. The size and shape control of nanoparticles using microwave energy rely on changing "classical" synthesis parameters like precursor concentration or precursor-to-additive ratio [28–30].

Antibacterial activity of TiO_2 nanoparticles has been described against several microorganisms [31,32,2], besides that contributing to the improvement of physical and mechanical properties [8,9,33]. According to Poosti et al. the addition of titanium oxide nanoparticles into an orthodontic composite resin can reduce enamel demineralization without compromising the physical properties [8]. Ahn et al. [34] also related similar results, showing that adhesive systems containing silver nanoparticles could prevent enamel demineralization around bracket surfaces without compromising physical properties.

The NPs used in this current study significantly decrease biofilm formation over the composite resin, however no differences were found between pure TiO_2 and Ag decorated NPs. However, previous studies reported the enhancement of antibacterial activity by synergistic effect between Ag and metal oxides, which could be mainly due to the increase on the generation of the reactive oxidative species (especially superoxide) and the increased damage to plasmid DNA induced by Ag doped NPs [17,18]. Bahadur et al. [15] also analyzed the effect of silver on the antibacterial properties of TiO_2. These authors studied the antibacterial, micro-structural, and fluorescence properties of Ag doped TiO_2 and showed that an excellent antibacterial performance was achieved using TiO_2 with an increasing concentration of Ag, as compared to the pure TiO_2, suggesting that antibacterial activity of nanoparticles remarkably enhances with increasing the Ag concentration in TiO_2. Obviously, the antibacterial effect of hybrids metal oxides and Ag depends on the concentration of silver. For dental applications, several types of Ag or Ag-ion containing fillers have been used such as Ag ion-implanted SiO_2, Ag-containing silica glass, Ag-zeolite, Ag-apatite, Ag-supported zirconium phosphate and Ag decorated metal oxides [4]. However, high concentrations of Ag into dental restorative materials could affect some properties, such as color stability and also can compromisse the homogeneous distribution into the composite resin. In this way, in our study we choose to create an Ag decoration of the previously synthesized NPs, using an aqueous silver solution. The use of silver decorated NPs synthesized by several chemical methods have been described, and the products were found to show high antimicrobial effect [5,35,36]. Zamperini et al. reported that Ag decorated hydroxyapatite nanospheres obtained by microwave-assited hydhotermal synthesis showed fungistatic and fungicidal effect against *C. albicans* planktonic cells and also exhibited antibiofilm activity, affecting mainly the extra-cellular matrix production [5]. The high antimicrobial capacity of Ag doped and decorated nanomaterials is mainly due to the enhancement of oxidative stress and the increased DNA damage induced by Ag containing NPs [17].

It is well know that a composite resin should have good mechanical properties besides the antibacterial activity, espe-

cially particularly in areas of high masticatory stresses [8,37]. In this way, the antibacterial activity provided by different agents should improve or at least no significant changes on mechanical properties is desired, for the acceptance as a successful dental restorative material. Our findings demonstrated a significant improvement of the compressive strength after inclusion of TiO_2 NPs (Fig. 9), probably due to surface treatment with organosilane agent. These results are similar to others studies, that modified a resin based restorative material with TiO_2 and showed the improvement for some properties such as the microhardness and flexural strength [38,39]. Organosilanes, as TEVS used in this current study, encourages further combination of the nanoparticles with the resin matrix, besides the improvement of the homogeneous distribution of the particles into a resin monomer [38,40]. Although, no difference was showed for diametral tensile strength as seen on Fig. 10.

The resin based restorative materials modified by antibacterial nanoparticles has has showed smoother surface roughness compared with the materials containing hybrid of nano and microsized fillers [41]. As previous reported, our findings also demonstrated that almost all modified Groups drastically increased the SR (Fig. 8). The increase of surface roughness could contribute to enhance *S. mutans* biofilm accumulation over the dental restorations, which can contributes to the secondary caries progression [41,3]. Otherwise, Ahn et al. [34] reported a significant low bacterial adhesion of cariogenic streptococci on the surface of experimental composite adhesives (ECAs) containing silica nanofillers and silver nanoparticles than conventional adhesives, although the ECAs had rougher surfaces than conventional adhesives due to the addition of silver nanoparticles. These authors concluded that ECAs can help prevent enamel demineralization around their surfaces without compromising physical properties.

The degree of conversion of modified composite resin remains unchanged after the inclusion of NPs into the composite resin, as demonstrated in Table 2. These data are in agreement with another study, which reported no significant differences on the degree of conversion after inclusion of small amounts of NPs into the composite resin [37]. Our results were also in agreement with Sun et al. [39] that reported an improvement of 3–7% on degree of conversion for a composite resin after inclusion of TiO_2 NPs. An increased degree of conversion is an important factor for a modified composite resin, since it could make a huge difference in terms of the number of crosslinks and polymer chain mobility, increasing the mechanical properties of the formed polymer.

In summary, this study showed that the inclusion of pure and Ag decorated TiO_2 into the composite resin can decrease *S. mutans* biofilm formation over the composite resin surface. An enhancement of mechanical properties was achieved after inclusion of TiO_2/Ag (PREC POL). The degree of conversion remains unchanging after modification with all tested NPs and the surface rougnhess was not significantly increased after inclusion of TiO_2/Ag (PREC POL). The TiO_2/Ag nanospheres obtained by polymeric precursor synthesis seems to be, among the tested NPs, the best nanomaterial to modifify the composite resin evaluated in this study.

Acknowledgement

The authors thank FAPEAM (Research Foundation of the Amazonas State, Amazonas, Brazil) for the financial support.

REFERENCES

[1] Ferracane JL. Resin composite — state of the art. Dent Mater 2011;27:29–38, http://dx.doi.org/10.1016/j.dental.2010.10.020.
[2] Chen L, Shen H, Suh BI. Antibacterial dental restorative materials: a state-of-the-art review. Am J Dent 2012;25:337–46.
[3] Nedeljkovic I, Teughels W, De Munck J, Van Meerbeek B, Van Landuyt KL. Is secondary caries with composites a material-based problem? Dent Mater 2015;31:e247–77, http://dx.doi.org/10.1016/j.dental.2015.09.001.
[4] Fan C, Chu L, Rawls HR, Norling BK, Cardenas HL, Whang K. Development of an antimicrobial resin — a pilot study. Dent Mater 2011;27:322–8, http://dx.doi.org/10.1016/j.dental.2010.11.008.
[5] Zamperini CA, André RS, Longo VM, Mima EG, Vergani CE, Machado AL, et al. Antifungal applications of Ag-decorated hydroxyapatite nanoparticles. J Nanomater 2013;2013, http://dx.doi.org/10.1155/2013/174398.
[6] Dias HB, Bernardi MIB, Ramos MA dos S, Trevisan TC, Bauab TM, Hernandes AC, et al. Zinc oxide 3D microstructures as an antimicrobial filler content for composite resins. Microsc Res Tech 2017:1–10, http://dx.doi.org/10.1002/jemt.22840.
[7] Tavassoli Hojati S, Alaghemand H, Hamze F, Ahmadian Babaki F, Rajab-Nia R, Rezvani MB, et al. Antibacterial, physical and mechanical properties of flowable resin composites containing zinc oxide nanoparticles. Dent Mater 2013;29:495–505, http://dx.doi.org/10.1016/j.dental.2013.03.011.
[8] Poosti M, Ramazanzadeh B, Zebarjad M, Javadzadeh P, Naderinasab M, Shakeri MT. Shear bond strength and antibacterial effects of orthodontic composite containing TiO_2 nanoparticles. Eur J Orthod 2013;35:676–9, http://dx.doi.org/10.1093/ejo/cjs073.
[9] Cai Y, Strømme M, Welch K. Photocatalytic antibacterial effects are maintained on resin-based TiO_2 nanocomposites after cessation of UV irradiation. PLoS One 2013;8, http://dx.doi.org/10.1371/journal.pone.0075929.
[10] Allaker RP. The use of nanoparticles to control oral biofilm formation. J Dent Res 2010;89:1175–86, http://dx.doi.org/10.1177/0022034510377794.
[11] Nel AE, Mädler L, Velegol D, Xia T, Hoek EMV, Somasundaran P, et al. Understanding biophysicochemical interactions at the nano-bio interface. Nat Mater 2009;8:543–57, http://dx.doi.org/10.1038/nmat2442.
[12] Sahu DR, Liu CP, Wang RC, Kuo CL, Huang JL. Growth and application of ZnO nanostructures. Int J Appl Ceram Technol 2013;10:814–38, http://dx.doi.org/10.1111/j.1744-7402.2012.02795.x.
[13] Hanaor DAH, Sorrell CC. Review of the anatase to rutile phase transformation. J Mater Sci 2011;46:855–74, http://dx.doi.org/10.1007/s10853-010-5113-0.
[14] Dwivedi C, Dutta V. Size controlled synthesis and photocatalytic activity of anatase TiO_2 hollow microspheres. Appl Surf Sci 2012;258:9584–8, http://dx.doi.org/10.1016/j.apsusc.2012.05.151.
[15] Bahadur J, Agrawal S, Panwar V, Parveen A, Pal K. Antibacterial properties of silver doped TiO_2 nanoparticles synthesized via sol–gel technique. Macromol Res 2016;24:488–93, http://dx.doi.org/10.1007/s13233-016-4066-9.

[16] Cai Y, Strømme M, Melhus A, Engqvist H, Welch K. Photocatalytic inactivation of biofilms on bioactive dental adhesives. J Biomed Mater Res B Appl Biomater 2014;102:62–7, http://dx.doi.org/10.1002/jbm.b.32980.
[17] Zhang Y, Gao X, Zhi L, Liu X, Jiang W, Sun Y, et al. The synergetic antibacterial activity of Ag islands on ZnO (Ag/ZnO) heterostructure nanoparticles and its mode of action. J Inorg Biochem 2014;130:74–83, http://dx.doi.org/10.1016/j.jinorgbio.2013.10.004.
[18] Ghosh S, Goudar VS, Padmalekha KG, Bhat SV, Indi SS, Vasan HN. ZnO/Ag nanohybrid: synthesis, characterization, synergistic antibacterial activity and its mechanism. RSC Adv 2012;2:930, http://dx.doi.org/10.1039/c1ra00815c.
[19] Chen YC, Chen LH, Min YL, Zhang YG. Simple method to synthesize novel mesoporous zinc oxide. J Mater Sci Mater Electron 2012;23:1759–63, http://dx.doi.org/10.1007/s10854-012-0658-0.
[20] Leite ER, Bernardi MIB, Longo E, Varela JA, Paskocimas CA. Enhanced electrical property of nanostructured Sb-doped SnO_2 thin film processed by soft chemical method. Thin Solid Films 2004;449:67–72, http://dx.doi.org/10.1016/j.tsf.2003.10.101.
[21] Walton RI. Subcritical solvothermal synthesis of condensed inorganic materials. Chem Soc Rev 2002;31:230–8, http://dx.doi.org/10.1039/b105762f.
[22] das Neves PBA, Agnelli JAM, Kurachi C, de Souza CWO. Addition of silver nanoparticles to composite resin: effect on physical and bactericidal properties in vitro. Braz Dent J 2014;25:141–5, http://dx.doi.org/10.1590/0103-6440201302398.
[23] Kasraei S, Sami L, Hendi S, Alikhani M-Y, Rezaei-Soufi L, Khamverdi Z. Antibacterial properties of composite resins incorporating silver and zinc oxide nanoparticles on *Streptococcus mutans* and *Lactobacillus*. Restor Dent Endod 2014;39:109–14, http://dx.doi.org/10.5395/rde.2014.39.2.109.
[24] Thommes M, Kaneko K, Neimark AV, Olivier JP, Rodriguez-Reinoso F, Rouquerol J, et al. Physisorption of gases, with special reference to the evaluation of surface area and pore size distribution (IUPAC technical report). Pure Appl Chem 2015;87:1051–69, http://dx.doi.org/10.1515/pac-2014-1117.
[25] Razavi RS, Loghman-estarki MR, Farhadi-khouzani M. Synthesis and characterization of ZnO nanostructures by polymeric precursor route. Acta Pol Phys A 2012;121:98–100.
[26] Bilecka I, Niederberger M. Microwave chemistry for inorganic nanomaterials synthesis. Nanoscale 2010;2:1358–74, http://dx.doi.org/10.1039/b9nr00377k.
[27] Jhung SH, Jin T, Hwang YK, Chang JS. Microwave effect in the fast synthesis of microporous materials: which stage between nucleation and crystal growth is accelerated by microwave irradiation? Chem A Eur J 2007;13:4410–7, http://dx.doi.org/10.1002/chem.200700098.
[28] He M, Jiu H, Liu Y, Tian Y, Li D, Sun Y, et al. Controllable synthesis of ZnO microstructures with morphologies from rods to disks. Mater Lett 2013;92:154–6, http://dx.doi.org/10.1016/j.matlet.2012.10.049.
[29] Aneesh PM, Vanaja KA, Jayaraj MK. Synthesis of ZnO nanoparticles by hydrothermal method. Nanosci Eng 2007;6639, http://dx.doi.org/10.1117/12.730364, 66390J-1.
[30] Moura KF, Maul J, Albuquerque AR, Casali GP, Longo E, Keyson D, et al. TiO_2 synthesized by microwave assisted solvothermal method: experimental and theoretical evaluation. J Solid State Chem 2014;210:171–7, http://dx.doi.org/10.1016/j.jssc.2013.11.023.
[31] Özyildiz F, Güden M, Uzel A, Karaboz I, Akil O, Bulut H. Antimicrobial activity of TiO_2-coated orthodontic ceramic brackets against *Streptococcus mutans* and *Candida albicans*. Biotechnol Bioprocess Eng 2010;15:680–5, http://dx.doi.org/10.1007/s12257-009-3005-4.
[32] Catauro M, Raucci M, Convertito C, Melisi D, Rimoli M. Characterization, bioactivity and ampicillin release kinetics of TiO_2 and TiO_24SiO_2 synthesized by sol–gel processing. J Mater Sci Mater Med 2006;17:413–20, http://dx.doi.org/10.1007/s10856-006-8468-7.
[33] Yu B, Ahn JS, Lim JI, Lee YK. Influence of TiO_2 nanoparticles on the optical properties of resin composites. Dent Mater 2009;25:1142–7, http://dx.doi.org/10.1016/j.dental.2009.03.012.
[34] Ahn SJ, Lee SJ, Kook JK, Lim BS. Experimental antimicrobial orthodontic adhesives using nanofillers and silver nanoparticles. Dent Mater 2009;25:206–13, http://dx.doi.org/10.1016/j.dental.2008.06.002.
[35] Peng J min, Lin J cheng, Chen Z yu, Wei M chao, Fu Y xiang, Lu S shen, sheng Yu D, Zhao W. Enhanced antimicrobial activities of silver-nanoparticle-decorated reduced graphene nanocomposites against oral pathogens. Mater Sci Eng C 2017;71:10–6, http://dx.doi.org/10.1016/j.msec.2016.09.070.
[36] Takahashi C, Matsubara N, Akachi Y, Ogawa N, Kalita G, Asaka T, et al. Visualization of silver-decorated poly (DL-lactide-*co*-glycolide) nanoparticles and their efficacy against *Staphylococcus epidermidis*. Mater Sci Eng C Mater Biol Appl 2017;72:143–9, http://dx.doi.org/10.1016/j.msec.2016.11.051.
[37] Tavassoli Hojati S, Alaghemand H, Hamze F, Ahmadian Babaki F, Rajab-Nia R, Rezvani MB, et al. Antibacterial, physical and mechanical properties of flowable resin composites containing zinc oxide nanoparticles. Dent Mater 2013;29:495–505, http://dx.doi.org/10.1016/j.dental.2013.03.011.
[38] Xia Y, Zhang F, Xie H, Gu N. Nanoparticle-reinforced resin-based dental composites. J Dent 2008;36:450–5, http://dx.doi.org/10.1016/j.jdent.2008.03.001.
[39] Sun J, Forster AM, Johnson PM, Eidelman N, Quinn G, Schumacher G, et al. Improving performance of dental resins by adding titanium dioxide nanoparticles. Dent Mater 2011;27:972–82, http://dx.doi.org/10.1016/j.dental.2011.06.003.
[40] Yang C, Yang C. Preparation of TiO_2 particles and surface silanization modification for electronic ink. J Mater Sci Mater Electron 2014;25:3285–9, http://dx.doi.org/10.1007/s10854-014-2015-y.
[41] Park JW, Song CW, Jung JH, Ahn SJ, Ferracane JL. The effects of surface roughness of composite resin on biofilm formation of *Streptococcus mutans* in the presence of saliva. Oper Dent 2012;37:532–9, http://dx.doi.org/10.2341/11-371-L.